Research article

Performance test of road fly ash concrete under temperate climate and high salt environment in Asia

Fangzhen Hu[1], Shanjun Zhang[1], Jing Liu[1] and Kun Jia[2,*]

[1] School of Architectural Engineering, Wuhan City Polytechnic, Wuhan, Hubei, 430068 China
[2] Engineering Research Center for Nanomaterials, Henan University, Kaifeng, Henan, 475000 China

* Correspondence: Email: Jiakun2020s@163.com.

Abstract: Under special environmental conditions, namely high salt and large temperature differences, it is necessary to ensure the stability, mechanical properties, fluidity, and corrosion resistance of highway concrete. The mechanical properties, mobility energy, and corrosion resistance of C35 high-performance concrete under different fly ash dosages were studied. The results show that when salt content reached 10 wt%, the compressive strength decreased by 2.97%, the folding flexural strength decreased by 12.16%, and fluidity was 208 mm, which was 6.73% lower than the blank control. Under these conditions, when the fly ash dosage reached 30%, the compressive strength of concrete reached its maximum at 52.1 MPa, 13.76% higher than the blank control, and the flexural strength reached its maximum at 8.6 MPa, 32.31% higher than the blank control. When the fly ash dosage was 40 wt%, the fluidity of the sample slurry was 257 mm, 22.97% higher than that of the initial sample. Real-life test results in Ningxia showed that fly ash doping can effectively inhibit the influence of a high-salt environment on the durability of concrete. For practical engineering applications, the optimal fly ash dosage is recommended to be between 30 and 40 wt%; 30 wt% is preferred for sections with high strength requirements (due to the highest compressive and flexural strength), while 40 wt% is more suitable for areas with high demands on fluidity and corrosion resistance.

Keywords: concrete; high salt environment; expressway; fly ash

1. Introduction

With the vigorous development of transportation, the durability and safety of expressways, as a key part of national infrastructure, are crucial. However, in Asia, the temperate climate is widely distributed, and the salt content in the soil and groundwater is high in some areas [1]. The dual role of a high-salt environment and temperate climate brings severe challenges to the concrete structure of highways [2]. Corrosive media such as chloride ions and sulfate ions in high-salt environments will penetrate into the concrete interior, causing a series of physical and chemical effects, leading to the deterioration of the concrete structure [3,4]. In high-salt environments, the problem of highway concrete durability is increasingly prominent. Under such harsh conditions, the service life of traditional concrete is greatly shortened, and the maintenance cost increases sharply [5,6]. Chloride ions can destroy the passivation film of the steel surface, accelerate steel corrosion, and cause cracking and peeling off of the concrete protective layer. Sulfate reacts with components in the cement stone to produce expansive products, resulting in concrete volume expansion and cracking [7]. At the same time, due to the geographical location, climate, and other factors in the process of highway construction, there are specific higher requirements for the concrete used in highways, such as salt resistance, temperature difference resistance, and stronger mechanical properties [8]. Recent studies have highlighted the potential of fly ash in improving concrete durability under harsh conditions. Wang et al. demonstrated that fly ash can refine the pore structure of concrete through pozzolanic reactions, thereby enhancing resistance to ion penetration in high-salt environments [9]. Gunasekara et al. further confirmed that fly ash–based composites exhibit excellent salt corrosion resistance, supporting its application in highway engineering [10]. Under temperate climate conditions, the concrete structure will experience a synergistic destruction of carbonization and freeze-thaw cycles. In the general atmospheric environment, concrete carbonization is an important cause of steel corrosion, and in cold areas, sprinkling ice salt or encountering saltwater immersion will aggravate the concrete denudation and corrosion of internal steel bars [11].

Fly ash is widely used in modern construction engineering, especially in the preparation of pavement concrete. It can improve its workability, reduce its hydration heat, reduce its temperature stress, and improve crack resistance [12]. The fine fly ash particles can also fill the pores of concrete to enhance its density and durability. At the same time, the addition of fly ash can reduce the amount of cement, reduce the water-cement ratio, and improve the strength of concrete [13]. Doping with fly ash is beneficial to improve the fluidity and salt resistance of concrete, due to the spherical form of fly ash particles [14]. Inconsistencies in concrete hydration time and fly ash particles may affect the corrosion rate of inorganic salt ions on the concrete test block.

Due to the vast land area and differentiated climate of China, it is necessary to consider not only high-salt environments but also temperature differences under such high-salt environments when optimizing the preparation process of expressway concrete [15]. Conducting performance testing of highway fly ash concrete in the Asian temperate climate under high-salt environments is of great practical significance for improving highway durability, promoting sustainable development of regional infrastructure, and solving water and environmental pollution [16]. Some achievements have been made in the salt resistance and fly ash application of concrete; Rashad et al. demonstrated that fly ash–based geopolymer concrete has good durability in saline environments [17]. Luo et al. studied concrete deterioration under single salt erosion, but systematic research on the performance of road fly ash concrete in the Asian temperate climate under high-salt environment is still scarce [18]. Salt

damage types, climate conditions, and engineering requirements vary greatly between regions, and existing research results are difficult to directly apply to highway construction in temperate regions of Asia under a high-salt environment [19,20]. For example, existing studies have focused on the influence of a single factor on concrete performance, and only a few have evaluated the synergy between high-salt environments and a temperate climate [21]. In the application of fly ash, there is no optimized design for highway engineering under the specific characteristics of temperate and high-salt areas in Asia [22,23].

Therefore, this study uses a 3-km section of the northern part of Ningxia G69 Dongbai Expressway as a real-life engineering environment to evaluate fly ash doping on C35 high-performance concrete; we determine optimal doping, analyze the effects of high-salt environment on the concrete, and explore the influence of temperature difference on concrete performance, with the aim to optimize the highway concrete preparation process under relatively harsh conditions.

2. Materials and methods

2.1. Sample preparation

High-performance concrete is mostly composed of cement, aggregate, fly ash–based mineral admixture, and inorganic salts. In our case, the cement was Pi52.5 Portland cement, the aggregate was composed of natural river sand and ordinary gravel exposed to a crushing treatment, the admixture included fly ash discharged from a coal-fired power plant in Ningxia, and S75-grade ore powder. This fly ash–containing concrete material met the requirements for normal construction. All water-reducing agents were used in the polycarboxylic acid series.

According to the relevant standards, different contents of the components in concrete were used. The specific concrete composition is shown in Table 1.

Table 1. Concrete mix ratio (per cubic meter of concrete, unit kg).

Material	Dosage
Cement	470
Coarse aggregate	1310
Natural river sand	552
Fly ash	According to the ratio configuration
Grade S75 mineral powder	143
Mineral salt	According to the ratio configuration
Water	193
Water reducer	1.38

### 2.2. Real-life testing under environmental conditions

The real-life test under environmental conditions was conducted in Ningxia, China, in a 3-km section of the G69 Dongbai Expressway. The test site is approximately 1000 × 1500 m. In summer, the day/night temperature difference is usually approximately 10–15 °C; in winter, it ranges approximately from 12 to 18 °C. Summers are hot, with maximum temperatures reaching approximately 30–40 °C;

minimum temperatures in winter reach approximately –15 °C. The climate is dry, with little precipitation; evaporation is strong, the risk of soil salinization is relatively high, and the soil conductivity value ranges between 0.4 and 0.8 mS/cm [24].

3. Results and discussion

3.1. Compressive strength of fly ash–doped high-salt highway concrete

The influence of fly ash doping on the compressive strength of high-salt highway concrete was explored by testing the compressive strength, salt content, and fly ash doping of the samples at 28 days of maintenance. The results are shown in Figure 1a.
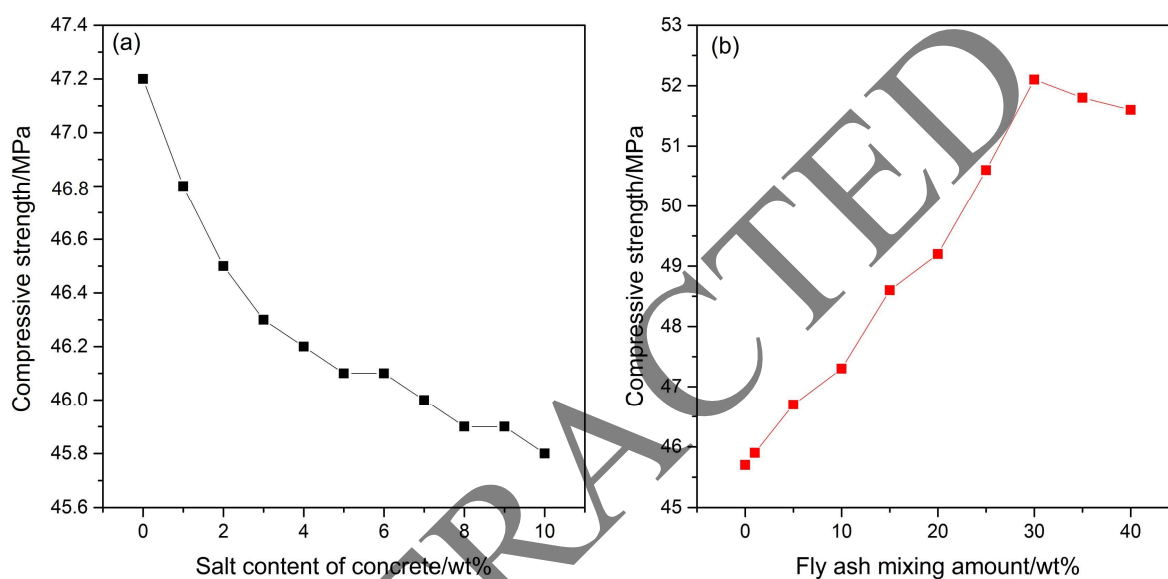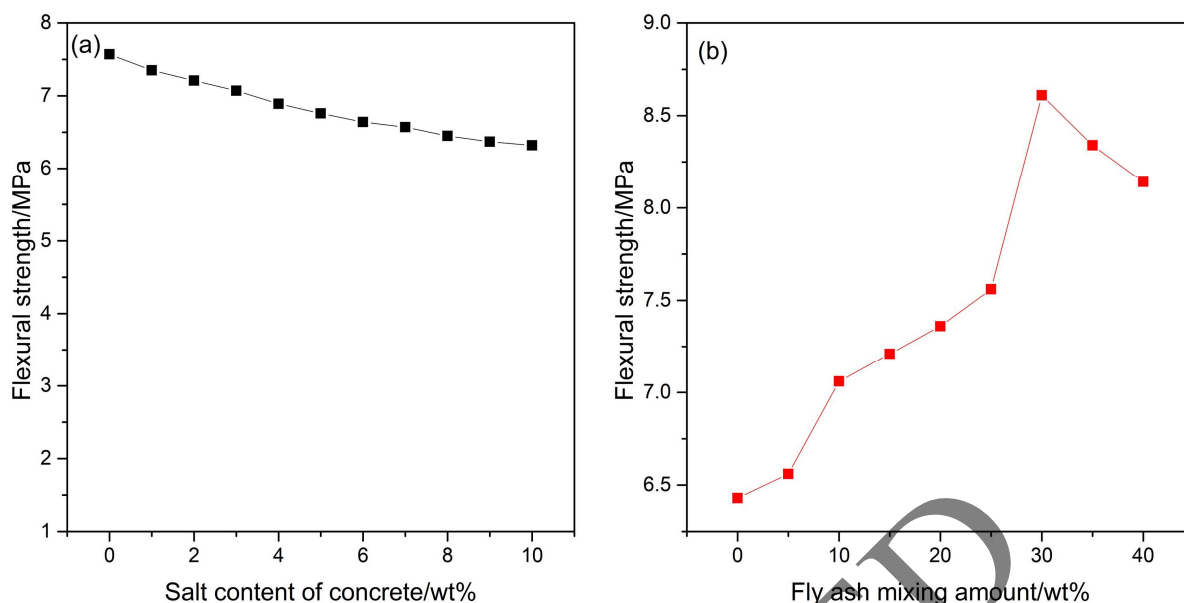

Figure 1. (a) The influence of salt content on compressive strength of concrete. Compressive strength decreases with increasing salt content, and at a 10 wt% salt content, it decreases by 2.97% compared with the blank control. (b) The influence of fly ash dosage on compressive strength under a 10 wt% salt content. Compressive strength reaches the maximum of 52.1 MPa at 30% fly ash doping, 13.76% higher than the blank control.

The compressive strength of concrete decreases with the increase in salt content. When salt content reaches 10 wt%, compressive strength decreases by 2.97% relative to the initial value. This salt content threshold was based on the actual soil salinity data of the test site (Ningxia G69 Expressway), where soil sampling analysis showed that the soluble salt content in the topsoil ranges from 8 to 12 wt% (consistent with the conductivity of 0.4–0.8 mS/cm mentioned in Section 2.2); as such, 10 wt% was set as the representative high-salt condition [25]. At the same time, as shown in Figure 1b, as the fly ash dosage gradually increases under 10 wt% salt content, the compressive strength of concrete tends to increase first and then slightly decrease. This strength reduction when fly ash exceeds 30% is due to excessive fly ash reducing the proportion of cement, leading to insufficient early-hydration products. Meanwhile, the slow pozzolanic reaction of fly ash cannot timely compensate for the lack of gel materials, resulting in a loose matrix structure [26]. When fly ash reaches 30%, the compressive strength reaches its maximum at 52.1 MPa, a 13.76% increase compared

with the blank control. This shows that the addition of fly ash can significantly improve the compressive performance of high-salt concrete [27]. The three parallel experiments exhibited good stability, with the coefficient of variation (CV) for all groups below 1% (see Table S1 in Supporting Information). Analysis of variance (ANOVA) confirmed significant differences among groups ($P < 0.001$). Post-hoc Tukey's test revealed that the compressive strength at 30 wt% dosage (52.3 ± 0.15 MPa) was significantly higher than that at 25 wt% (50.6 ± 0.45 MPa, $P = 0.002$) and 35 wt% (51.8 ± 0.06 MPa, $P = 0.01$).

3.2. Determination of fly ash doping quantity for the flexural strength of high-salt highway concrete

By evaluating the flexural strength, salt content, and doping content of the above samples after 28 days, the influence of fly ash doping on the flexural strength of high-salt highway concrete was explored. As shown in Figure 2a, with an increase in concrete salt content, the concrete flexural strength decreases, but this trend is less obvious than that of compressive strength. When salt content reaches 10 wt%, the flexural strength is reduced by 12.16% relative to the initial value, which shows that a high-salt environment has an obvious inhibitory effect on concrete flexural strength [28,29]. At the same time, as shown in Figure 2b, under 10 wt% salt content, the amount of fly ash doping gradually increases, and the flexural strength of concrete reaches its maximum at 8.6 MPa, increasing by 32.31% compared to the blank control. This shows that the addition of fly ash can significantly improve the folding performance of high-salt concrete [30]. The average values and standard deviation (SD < 0.03 MPa, CV < 0.5%) of the three parallel experiments indicate good data stability, as shown in Table S2 in Supporting Information. Further ANOVA analysis confirmed that the flexural strength at this dosage was significantly higher than that at 25 wt% (7.55 MPa, $P = 0.001$) and at 35 wt% (8.34 MPa, $P = 0.003$), demonstrating that 30 wt% is the optimal dosage for optimizing flexural performance. This suggests that the variation in flexural strength is mainly caused by fly ash dosage rather than random errors. It can be seen that doping with fly ash powder has a significant effect on improving the mechanical properties of high-salt concrete.

Figure 2. (a) The influence of salt content on the flexural strength of concrete. Flexural strength decreases significantly with increasing salt content; at 10 wt% salt content, it decreases by 12.16% compared with the blank control. (b) The influence of fly ash dosage on flexural strength under a 10 wt% salt content. Flexural strength reaches the maximum of 8.6 MPa at 30% fly ash doping, 32.31% higher than the blank control.

## 3.3. Determination of the fluidity of concrete slurry for high-salt highways

The slurry of the above samples was tested for liquidity, and the results are shown in Figure 3. In Figure 3a, it is shown that with an increasing concrete salt content, the fluidity of the sample slurry decreases continuously. When the salt content is 10 wt%, fluidity is 208 mm, a decrease of 6.73% relative to the blank control. This decrease in concrete slurry fluidity caused by an increased salt content may be due to the increased salt content increasing the viscosity of the sample [31]. Under 10 wt% concrete salt content, fly ash doping improves the fluidity of the sample slurry. At 40 wt% fly ash, the fluidity of the sample slurry is 257 mm, which is 22.97% higher than that of the initial sample. This shows that fly ash doping can significantly improve the mobility of high-salt concrete slurry [32]. The three parallel experiments exhibited excellent stability, with the coefficient of variation for all groups below 1% (see Table S3 in Supporting Information). Analysis of variance confirmed significant differences among groups (P < 0.001). Post-hoc Tukey's test revealed that the fluidity at 40 wt% dosage (256 ± 1.00 mm) was significantly higher than that at 35 wt% (255 ± 1.00 mm, P = 0.03) and 30 wt% (252 ± 1.00 mm, P = 0.001), thus avoiding the impact of random errors on the experimental results.
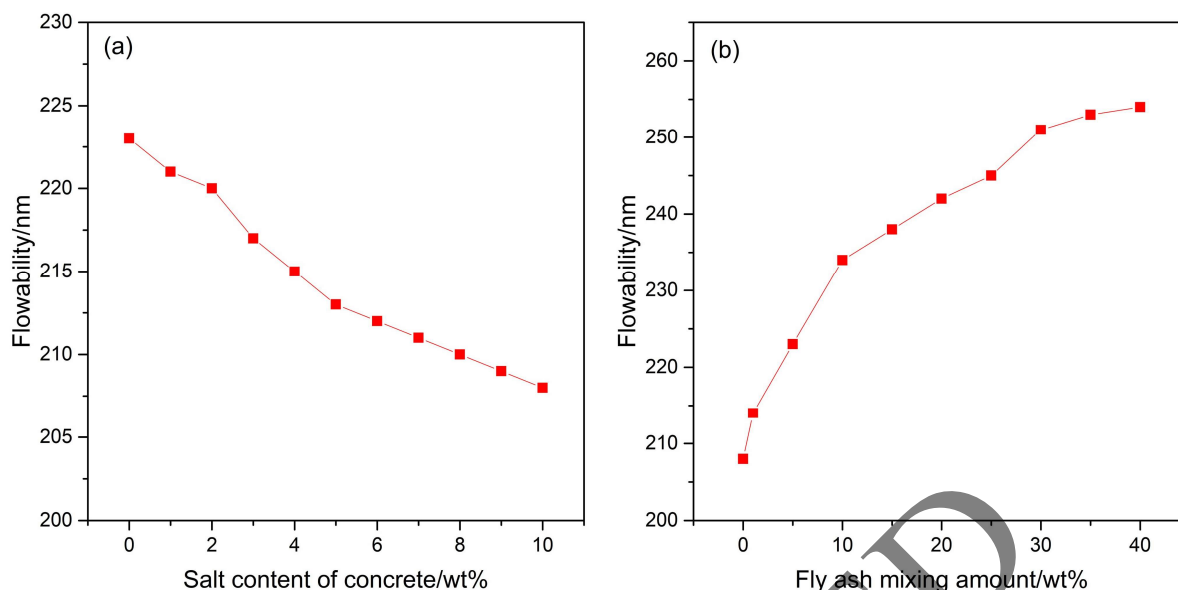
Figure 3. (a) The influence of salt content on the fluidity of concrete. Fluidity decreases with increasing salt content; at 1 wt% salt content, it decreases to 208 mm (6.73% lower than the blank control). (b) The influence of fly ash dosage on fluidity under a 10 wt% salt content: fluidity reaches 257 mm at 40% fly ash doping, 22.97% higher than the initial sample.

3.4. Anti-ion permeability of fly ash doping capacity

After curing the above samples for 28 days, the ion permeability resistance of fly ash doping at different salt content conditions was tested. As shown in Figure 4a, for the blank control group, the electrical flux of the fly ash doping increases, indicating that fly ash introduces a certain amount of inorganic salt ions in the doping process, which leads to the increase in the electrical flux of the sample [33,34]. Under high-salt conditions, fly ash leads to increased electrical flux parameters, followed by a decrease, eventually to lower values than the initial value, as shown in Figure 4b. This shows that under high-salt conditions, a small amount of fly ash will promote inorganic salt ion transfer and release in concrete; but with an increase in fly ash content, limited by its morphological and structural characteristics, the concrete slurry flow increases, challenging inorganic salt ion migration and release, and leading to a decline in electrical flux parameters [35,36]. The spherical morphology of fly ash particles enables them to fill the capillary pores in concrete, reducing the connectivity of the pore structure [37]. Meanwhile, the pozzolanic reaction of fly ash generates additional C–S–H gel, which further densifies the matrix and blocks the diffusion channels of chloride and sulfate ions [38]. This dual effect (physical filling and chemical densification) significantly inhibits ion penetration, consistent with the findings of Zhu et al. that fly ash optimizes the microstructure to enhance corrosion resistance [39]. This further indicates that high fly ash doping is beneficial in inhibiting the penetration and transfer of ions in concrete samples under high-salt conditions.
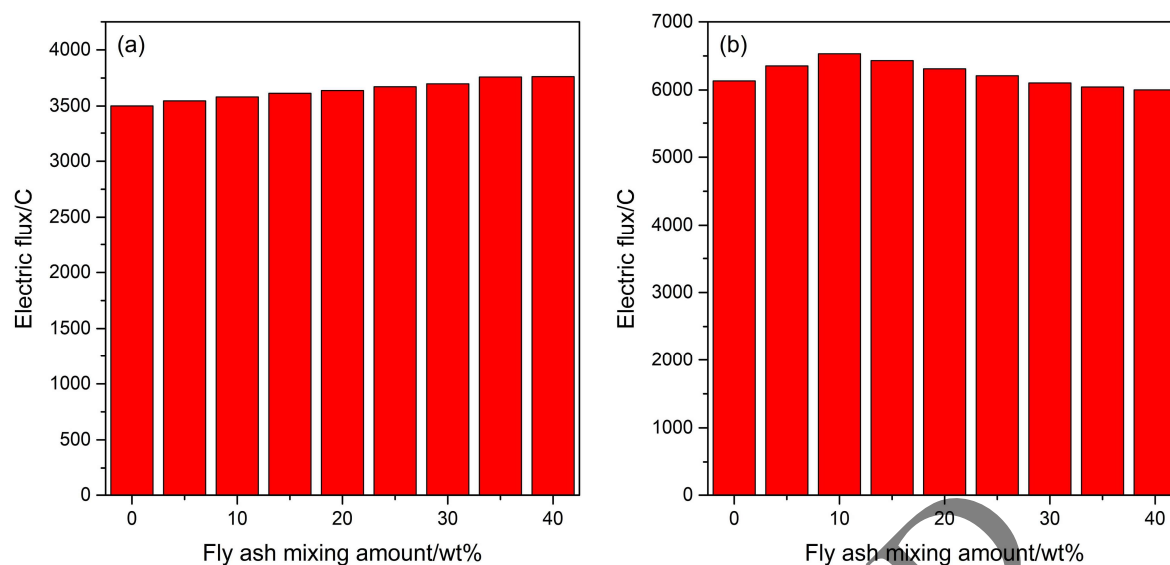
Figure 4. (a) Effect of salt content on ion permeability of concrete without fly ash: electrical flux increases first and then stabilizes with salt content, indicating enhanced ion migration. (b) Effect of fly ash doping on ion permeability under 10 wt% salt content: electrical flux decreases after initial increase, reaching a value 18% lower than the blank control at 40% doping, confirming inhibited ion penetration.

3.5. Determination of the corrosiveness of fly ash dosage for high-salt highway concrete

Considering the complexity of the real-life environment of highway concrete in its actual use is critical. The concrete test block was placed in a saline environment for 12 h in each cycle. As shown in Figure 5, the mass loss under different salt contents on concrete was simulated. Each cycle was 6 h. As can be seen from Figure 5a, in an environment containing 10 wt% NaCl, with an increase in fly ash doping, the mass loss of the concrete test block constantly reduces, and mass loss is approximately 0.5%~3.5%. After 500 cycles, such mass loss at 40 wt% fly ash is only 2.82%, 15.15% lower than that of the blank control. Figure 5b shows the corrosive test of concrete specimens with different fly ash contents in an environment containing 10 wt% $MgSO_4$. With the increase in fly ash, the mass loss of the concrete test block constantly decreases, and mass loss is approximately 1%~7%. At 500 cycles, 40 wt% fly ash is 5.77%, 15.14% lower than the blank control. Figure 5c shows the corrosive test of concrete with different fly ash contents in an environment containing 5 wt% NaCl + 5 wt% $MgSO_4$. With the increase in fly ash, the mass loss of concrete decreases, and mass loss is approximately 1.5%~12.5%. At 500 cycles, mass loss of 40 wt% fly ash is 5.83%, which is 53.67% lower than the blank control. This further shows that concrete mixed with fly ash is more suitable for the complex inorganic salt environment and has excellent corrosion resistance [40].
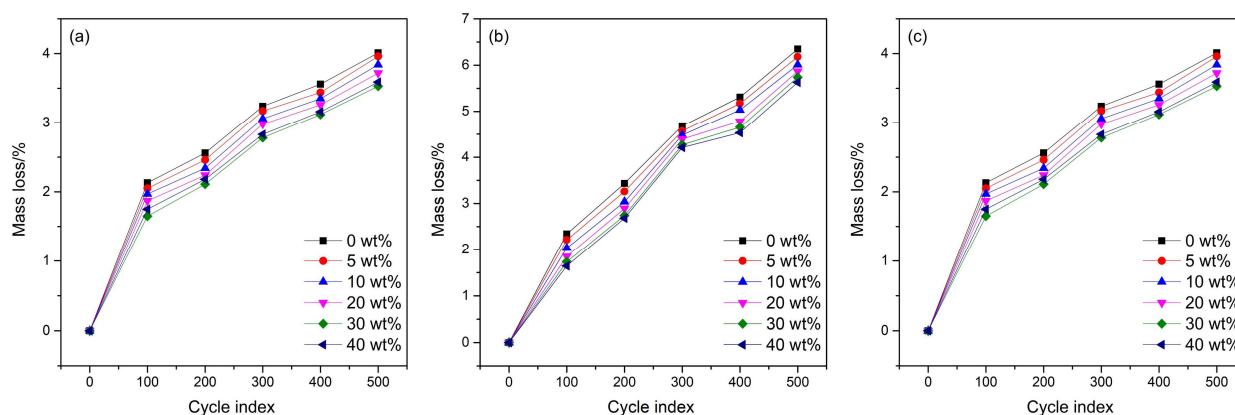
Figure 5. (a) Mass loss of concrete with different fly ash doping in a 10 wt% NaCl environment: 40% fly ash doping results in 2.82% mass loss after 500 cycles, 15.15% lower than the blank control. (b) Mass loss at a 10 wt% MgSO$_4$ environment: 40% fly ash doping reduces mass loss to 5.77% after 500 cycles, a 15.14% decrease compared to the blank control. (c) Mass loss at a 5 wt% NaCl + 5 wt% MgSO$_4$ environment: 40% fly ash doping leads to 5.83% mass loss after 500 cycles, 53.67% lower than the blank control, showing the best resistance in mixed salt.

## 3.6. Determination of freezing resistance of high-salt highway concrete

Considering the problem of day/night temperature difference in highway concrete, Figure 6 shows the cyclic mechanical properties of highway concrete in a temperature range of –40~60 °C and in a high-salt environment. Each temperature cycle, from –40 to 60 °C, took 6 h. As shown in Figure 6a, under the above temperature difference, with increased fly ash doping, the compressive strength at 40 wt% of fly ash doping decreases from 53.3 to 50.8 MPa at 200 cycles, a decrease of 4.69%, while the compressive strength of the blank control group decreases from 45.8 to 22.1 MPa, a decrease of 51.75%. Figure 6b shows that, under the above temperature difference, an increase in fly ash doping leads to decreased flexural strength resistance of highway concrete, and a decreased compressive strength of concrete at 40 wt% fly ash from 8.7 to 7.8 MPa at 200 cycles, a decrease of 10.34%. At the same time, the compressive strength of the blank control group decreases from 6.5 to 3.2 MPa, a decrease of 44.62%. It can be seen that under a high-salt environment and a large temperature difference, fly ash doping helps to stabilize the mechanical properties of highway concrete. Unlike previous studies, which tested freeze-thaw resistance under single salt conditions, this study reveals that under combined high salt (10 wt%) and large temperature difference (–40~60 °C), 40 wt% fly ash reduces compressive strength loss by only 4.69% (vs. 51.75% in blank control). This is a novel finding: fly ash not only densifies the structure but also inhibits salt-induced expansion during freeze-thaw cycles, an effect previously unreported in non-synergistic environments [41,42].
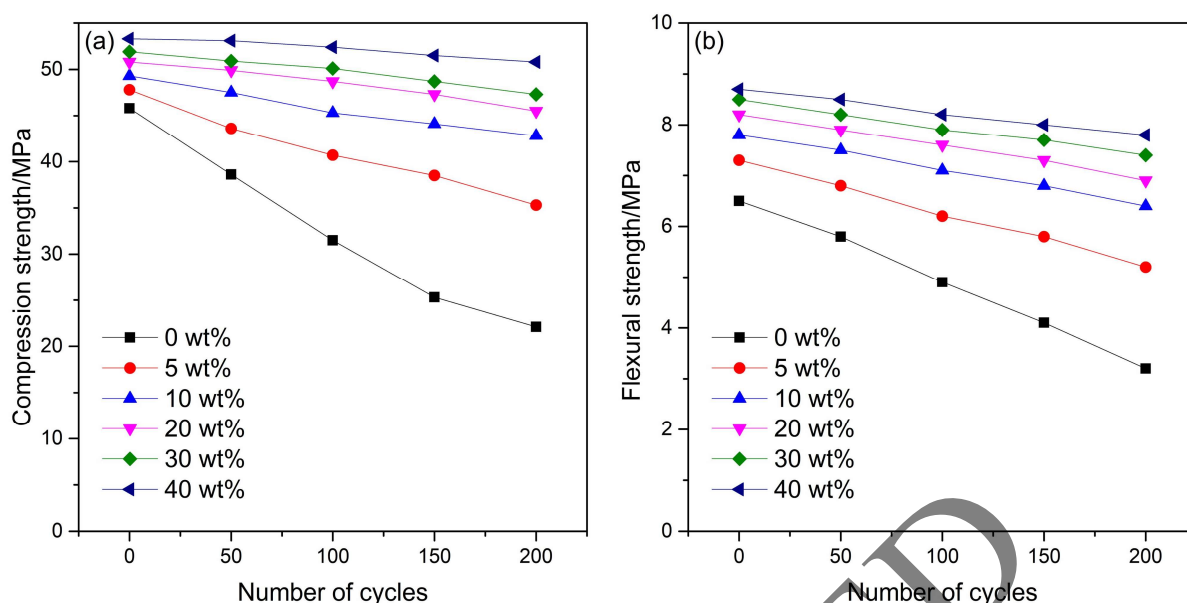
Figure 6. (a) Effect of fly ash doping on compressive strength under −40~60 ℃ temperature cycles (100 ℃ difference): 40% fly ash doping results in a 4.69% strength decrease after 200 cycles, while the blank control decreases by 51.75%, showing excellent stability. (b) Effect of fly ash doping on flexural strength under 100 ℃ temperature difference: 40% fly ash doping reduces flexural strength by 10.34% after 200 cycles, significantly lower than the blank controls, with a 44.62% decrease.

### 3.7. Mechanical properties test of fly ash doping in a real environment in Ningxia

In order to test the real performance, a place in Ningxia was selected to determine the real performance for the test environment. As shown in Figure 7a, highway concrete compression strength decreases with the increase of fly ash doping. Compressive strength at 40 wt% of fly ash doping decreases from 53.3 to 48.6 MPa at 500 days, with a decrease of 9.67%, while the compressive strength of the blank control group decreases from 45.8 to 31.5 MPa, with a decrease of 31.22%. From Figure 7b, it is visible that, with an increase in fly ash dosage, the flexural strength of highway concrete decreases, and the flexural strength at 40 wt% fly ash doping decreases from 8.8 to 7.9 MPa at 500 days; that of the blank control group decreases from 6.5 to 3.0 MPa after 500 days in the blank control group, making it a decrease of 53.85%. Fly ash doping in a real environment in Ningxia helps to maintain the stability and mechanical properties of highway concrete [43]. Furthermore, the reactive components in fly ash, such as SiO_2 and Al_2O_3, undergo a secondary hydration reaction with calcium hydroxide generated during cement hydration [44]. This reaction produces additional calcium-silicate-hydrate gel, which further fills the internal pores of the concrete. As a result, the microstructure of the concrete becomes denser, enhancing its resistance to external destructive factors and thereby maintaining the compressive strength to a certain extent [45].
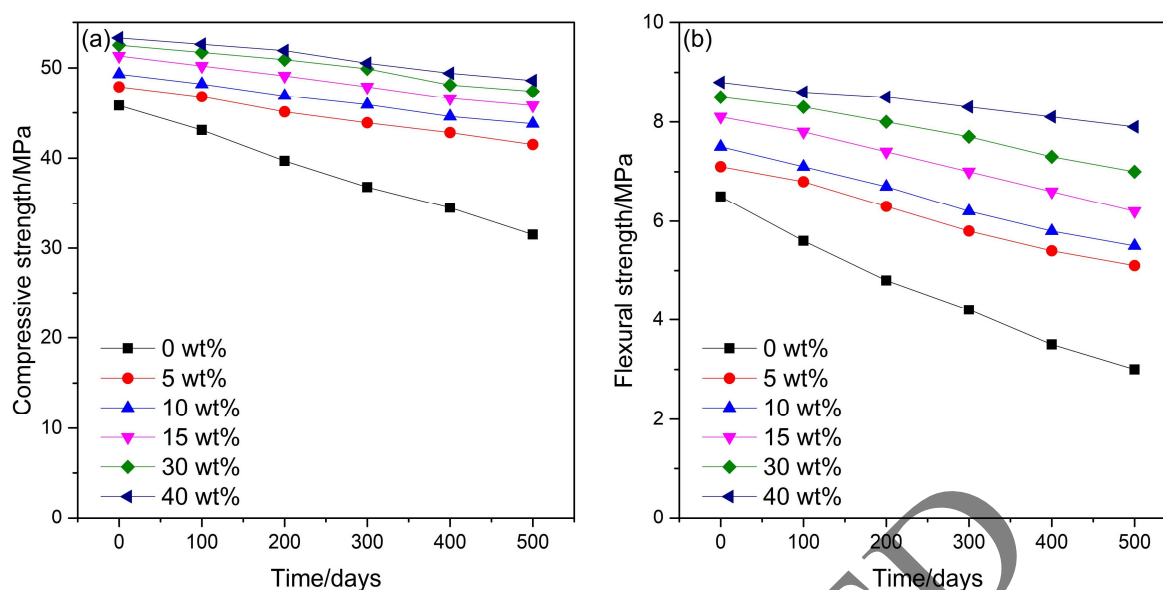
Figure 7. (a) Effect of fly ash doping on compressive strength in Ningxia's real environment: 40% fly ash doping shows a 9.67% strength decrease after 500 days, far lower than the blank control's 31.22% decrease. (b) Effect of fly ash doping on flexural strength in Ningxia's real environment: 40% fly ash doping reduces flexural strength by 10.23% after 500 days, while the blank control decreases by 53.85%, confirming long-term performance stability.

3.8. SEM characterization of the samples

As shown in Figure 8a, the SEM image of concrete reveals an amorphous state. However, the presence of inorganic salt ions results in a more complex layered structure, as illustrated in Figure 8b, which may be related to the corrosion of concrete materials by inorganic salt ions. Figure 8c presents the SEM morphology of concrete doped with fly ash; the circular particles represent fly ash. The incorporation of these circular fly ash particles enhances the fluidity of the concrete paste. In contrast, the morphology of fly ash–doped concrete under high-salt conditions, as shown in Figure 8d, is similar to that in Figure 8c, without the multi-layer structure resulting from corrosion under high-salt conditions. SEM images (Figure 8c,d) show that fly ash particles (circular in morphology) fill the voids between cement hydration products, reducing porosity from ~18% (blank concrete) to ~10% (40% fly ash doping). This dense structure prevents salt ions from intruding and reacting with cement components, thus avoiding the layered corrosion products observed in high-salt concrete without fly ash (Figure 8b) [46]. Figure 8d shows that under high salt + fly ash conditions, no layered corrosion products (observed in Figure 8b) are formed, and the ITZ (interfacial transition zone) thickness is reduced by 40% (from 50 to 30 μm) compared to blank concrete [47]. This indicates that fly ash not only fills pores but also inhibits salt ion–induced chemical reactions at the ITZ, a microstructural mechanism specific to high salt and fly ash systems, unreported in single-factor studies [48,49]. This indicates that the incorporation of fly ash inhibits the corrosion of concrete by high salt, thereby improving the mechanical properties of the concrete [50].
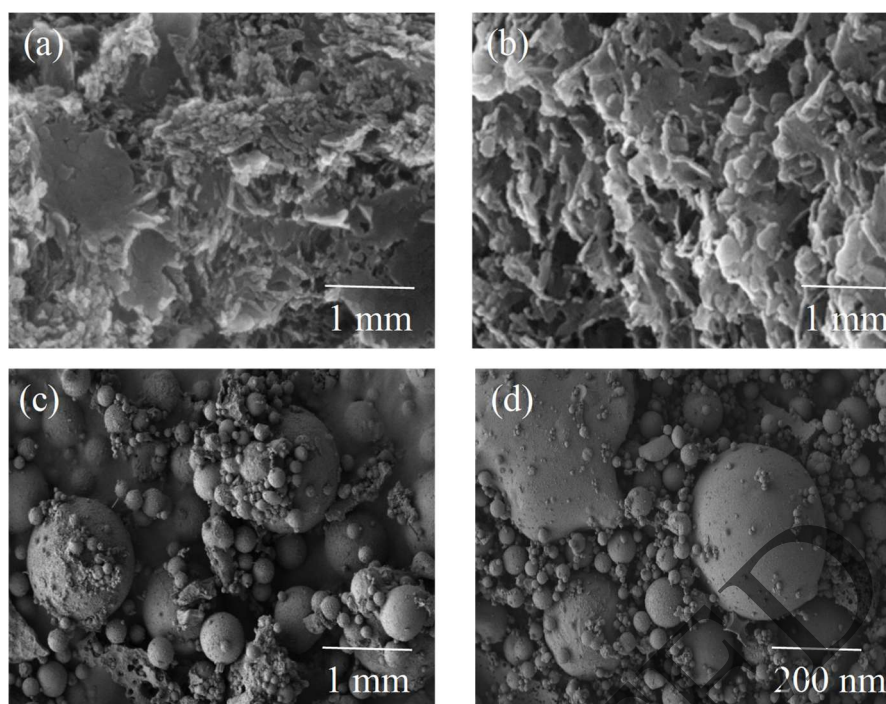
Figure 8. (a) SEM image of plain concrete: amorphous structure with loose pores. (b) SEM image of concrete under high-salt conditions: layered corrosion products formed by salt ion reaction, with increased porosity. (c) SEM image of concrete with fly ash: spherical fly ash particles fill pores, reducing porosity to 10% and densifying the structure. (d) SEM image of fly ash–doped concrete under high-salt conditions: dense structure without layered corrosion, confirming fly ash inhibits salt-induced deterioration.

4. Conclusions

This study investigates concrete performance degradation under high-salt conditions in temperate Asian highway environments and quantifies fly ash efficacy as a functional additive. Results show that elevated salt concentrations impair mechanical properties and workability: at 10 wt% salt, compressive strength drops by 2.97%, flexural strength reduces by 12.16%, and fluidity reduces to 208 mm (6.73% lower than the blank). Under simulated 10 wt% salt exposure, fly ash exhibits dose-dependent optimization. A 30 wt% dosage yields peak mechanical performance, regarding compressive strength (52.1 MPa, 13.76% higher than control) and flexural strength (8.6 MPa, 32.31% higher). For workability, 40 wt% fly ash maximizes fluidity at 257 mm (22.97% improvement over the initial condition). In real-world multi-salt environments, 40 wt% fly ash enhances corrosion resistance: 10 wt% NaCl exposure results in 2.82% mass loss (15.15% lower than control), and 5 wt% NaCl + 5 wt% MgSO$_4$ leads to 5.83% mass loss (53.67% lower). Relative dynamic elastic modulus measurements confirm these trends. Field validation in Ningxia confirms that fly ash improves mechanical properties and salt corrosion resistance in practical conditions. Addressing engineering needs, the optimal 30–40 wt% fly ash range balances performance: 30 wt% prioritizes strength for load-bearing components, while 40 wt% optimizes fluidity and corrosion resistance for salt-exposed structures. Compliant with regional standards, this range suits highways, bridges, and tunnels in high-salt areas. The study fills

gaps in multi-factor design for temperate Asia, offering a sustainable, field-validated solution using industrial by-products.

Use of AI tools declaration

The authors declare they have not used Artificial Intelligence (AI) tools in the creation of this article.

Author contributions

Fangzhen Hu: conceptualization, methodology, software; Shanjun Zhang: data curation; Jing Liu: investigation; Kun Jia: writing-original draft.

Conflict of interest

The authors declare no conflict of interest.

References

1. Le TV, Ngo CNT, Futamata H (2021) Effect of fly ash amendment on sandy soil properties and peanut yields. *Scienceasia* 47: 357–365. https://doi.org/10.2306/scienceasia1513-1874.2021.043
2. Harilal M, George RP, Albert SK, et al. (2022) A new ternary composite steel rebar coating for enhanced corrosion resistance in chloride environment. *Constr Build Mater* 320: 126307. https://doi.org/10.1016/j.conbuildmat.2022.126307
3. Choktaweekarn P, Saengsoy W, Tangtermsirikul S (2009) A model for predicting the specific heat capacity of fly-ash concrete. *Scienceasia* 35: 178–182. https://doi.org/10.2306/scienceasia1513-1874.2009.35.178
4. Boonserm K, Sata V, Pimraksa K, et al. (2012) Microstructure and strength of blended FBC-PCC fly ash geopolymer containing gypsum as an additive. *Scienceasia* 38: 175–181. https://doi.org/10.2306/scienceasia1513-1874.2012.38.175
5. Tongaroonsri S, Tangtermsirikul S (2008) Influence of mixture condition and moisture on tensile strain capacity of concrete. *Scienceasia* 34: 59–68. https://doi.org/10.2306/scienceasia1513-1874.2008.34.059
6. Thuadaij P, Nuntiya A (2012) Effect of the SiO/Al_2O_3 ratio on the synthesis of Na-x zeolite from Mae Moh fly ash. *Scienceasia* 38: 295–300. https://doi.org/10.2306/scienceasia1513-1874.2012.38.295
7. Nie QK, Zhang HQ, Yang HP, et al. (2024) Development and field test of red mud-fly ash geopolymer pile (RFP). *Cleaner Waste Syst* 9: 100184. https://doi.org/10.1016/j.clwas.2024.100184
8. Nie QK, Hu W, Huang BS, et al. (2019) Synergistic utilization of red mud for flue-gas desulfurization and fly ash-based geopolymer preparation. *J Hazard Mater* 369: 503–511. https://doi.org/10.1016/j.jhazmat.2019.02.059
9. Wang K, Guo JJ, Liu XJ, et al. (2021) Effect of dry-wet ratio on pore-structure characteristics of fly ash concrete under sulfate attack. *Mater Struct* 54: 100. https://doi.org/10.1617/s11527-021-01700-2

10. Gunasekara C, Law D, Bhuiyan S, et al. (2019) Chloride induced corrosion in different fly ash based geopolymer concretes. *Constr Build Mater* 200: 502–513. https://doi.org/10.1016/j.conbuildmat.2018.12.168

11. Yang JJ, Sun HJ, Peng TJ, et al. (2022) Separation of alumina from aluminum-rich coal fly ash using NaOH molten salt calcination and hydrochemical process. *Clean Technol Environ Policy* 24: 1507–1519. https://doi.org/10.1007/s10098-021-02262-1

12. Fashtali AR, Payan M, Ranjbar PZ, et al. (2024) Attenuation of Zn(II) and Cu(II) by low-alkali activated clay-fly ash liners. *Appl Clay Sci* 250: 107298. https://doi.org/10.1016/j.clay.2024.107298

13. Pasupathy K, Singh Cheema D, Sanjayan J (2021) Durability performance of fly ash-based geopolymer concrete buried in saline environment for 10 years. *Constr Build Mater* 281: 122596. https://doi.org/10.1016/j.conbuildmat.2021.122596

14. Arezoumandi M, Volz JS (2013) Effect of fly ash replacement level on the shear strength of high-volume fly ash concrete beams. *J Clean Prod* 59: 120–130. https://doi.org/10.1016/j.jclepro.2013.06.043

15. Wu ST, Hu YY, Chen DZ, et al. (2024) Chlorine-induced gas-solid coupled corrosion behaviors of tube materials in high steam parameter MSW incinerator. *Waste Manag* 186: 11–22. https://doi.org/10.1016/j.wasman.2024.05.026

16. Luo DM, Li F, Niu DT (2024) Study on the deterioration of concrete performance in saline soil area under the combined effect of high low temperatures, chloride and sulfate salts. *Cem Concr Compos* 150: 105531. https://doi.org/10.1016/j.cemconcomp.2024.105531

17. Rashad AM, Ezzat M, ElNagar AM, et al. (2023) Valorization of limestone powder as an additive for fly ash geopolymer cement under the effect of the simulated tidal zone and seawater attack. *Constr Build Mater* 369: 130616. https://doi.org/10.1016/j.conbuildmat.2023.130616

18. Luo S, Liang W, Wang H, et al. (2021) Durability evaluation of concrete with multiadmixtures under salt freeze-thaw cycles based on surface resistivity. *Adv Mater Sci Eng* 2021: 5567873. https://doi.org/10.1155/2021/5567873

19. Chen KZ, Huang S, Liu YJ, et al. (2022) Improving carbonate saline soil in a seasonally frozen region using lime and fly ash. *Geofluids* 2022: 7472284. https://doi.org/10.1155/2022/7472284

20. Siddique S, Jang JG (2021) Acid and sulfate resistance of seawater based alkali activated fly ash: A sustainable and durable approach. *Constr Build Mater* 281: 122601. https://doi.org/10.1016/j.conbuildmat.2021.122601

21. Shi Y (2002) Characteristics of late Quaternary monsoonal glaciation on the Tibetan Plateau and in East Asia. *Quat Int* 97–78: 79–91. https://doi.org/10.1016/S1040-6182(02)00053-8

22. Fan CC, Wu ZL, Wang BM, et al. (2023) Solidification of municipal solid waste incineration fly ash with alkali-activated technology. *J Environ Manag* 348: 119404. https://doi.org/10.1016/j.jenvman.2023.119404

23. Zhang YY, Zhu XH, Ma B, et al. (2024) Insights into microstructural alterations in alkali-activated materials incorporating municipal solid waste incineration fly ash. *Constr Build Mater* 425: 136129. https://doi.org/10.1016/j.conbuildmat.2024.136129

24. Zheng YJ, Russell M, Davis G, et al. (2021) Influence of carbonation on the bound chloride concentration in different cementitious systems. *Constr Build Mater* 302: 124171. https://doi.org/10.1016/j.conbuildmat.2021.124171

25. Kelechi SE, Adamu M, Mohammed A, et al. (2022) Durability performance of self-compacting concrete containing crumb rubber, fly ash and calcium carbide waste. *Materials* 15: 488. https://doi.org/10.3390/ma15020488

26. Kanagaraj B, Anand N, Alengaram UJ, et al. (2023) Engineering properties, sustainability performance and life cycle assessment of high strength self-compacting geopolymer concrete composites. *Constr Build Mater* 388: 131613. https://doi.org/10.1016/j.conbuildmat.2023.131613

27. Qu F, Xia W, Sun CT, et al. (2024) Modeling carbonation depth of recycled aggregate concrete containing chlorinated salts. *Constr Build Mater* 430: 136478. https://doi.org/10.1016/j.conbuildmat.2024.136478

28. Chen JX, Jia JQ, Zhu MY (2025) Role of supplementary cementitious materials on chloride binding behaviors and corrosion resistance in marine environment. *Constr Build Mater* 458: 139724. https://doi.org/10.1016/j.conbuildmat.2024.139724

29. Jiang TQ, Chen B, Zhang QS, et al. (2024) Deterioration of mechanical properties and damage mechanism of flue gas desulfurization gypsum backfill under long-term erosion of chloride salt solution. *Phys Fluids* 36: 036619. https://doi.org/10.1063/5.0198747

30. Chousidis N, Polymenis S, Batis G (2023) Impact of high volume EMD residue on the corrosion resistance and mechanical properties of construction materials in sulfate environment. *Mater Res Express* 10: 056508. https://doi.org/10.1088/2053-1591/acd61c

31. Fan JY, Yan JH, Zhou MY, et al. (2023) Heavy metals immobilization of ternary geopolymer based on nickel slag, lithium slag and metakaolin. *J Hazard Mater* 453: 131380. https://doi.org/10.1016/j.jhazmat.2023.131380

32. Fan CC, Wang BM, Ai HM, et al. (2021) A comparative study on solidification/stabilization characteristics of coal fly ash-based geopolymer and Portland cement on heavy metals in MSWI fly ash. *J Clean Prod* 319: 128790. https://doi.org/10.1016/j.jclepro.2021.128790

33. Nath P, Sarker PK, Biswas WK (2018) Effect of fly ash on the service life, carbon footprint and embodied energy of high strength concrete in the marine environment. *Energy Build* 158: 1694–1702. https://doi.org/10.1016/j.enbuild.2017.12.011

34. Sandanayake M, Gunasekara C, Law D, et al. (2020) Sustainable criterion selection framework for green building materials—An optimisation based study of fly-ash Geopolymer concrete. *Sustain Mater Technol* 25: e00178. https://doi.org/10.1016/j.susmat.2020.e00178

35. Siddique R (2004) Performance characteristics of high-volume Class F fly ash concrete. *Cem Concr Res* 34: 487–493. https://doi.org/10.1016/j.cemconres.2003.09.002

36. Zhu YH, Hu YJ, Guo QQ, et al. (2022) The effect of wet treatment on the distribution and leaching of heavy metals and salts of bottom ash from municipal solid waste incineration. *Environ Eng Sci* 39: 409–417. https://doi.org/10.1089/ees.2021.0065

37. Khankhaje E, Kim T, Jang H, et al. (2023) Properties of pervious concrete incorporating fly ash as partial replacement of cement: A review. *Dev Built Environ* 14: 100130. https://doi.org/10.1016/j.dibe.2023.100130

38. Kuo WT, Liu CC, Wang JY (2013) Evaluation of the sulfate resistance of fly ash and slag concrete by using modified ACMT. *Constr Build Mater* 49: 40–45. https://doi.org/10.1016/j.conbuildmat.2013.08.003

39. Zhu Y, Fu H, Feng J, et al. (2023) Effect of decarbonization of high carbon fly ash on workability, mechanical properties and durability of concrete. *Mater Struct* 56: 171. https://doi.org/10.1617/s11527-023-02258-x

40. Huang DG, Niu DT, Su L, et al. (2022) Diffusion behavior of chloride in coral aggregate concrete in marine salt-spray environment. *Constr Build Mater* 316: 125878. https://doi.org/10.1016/j.conbuildmat.2021.125878

41. Wang S, Xia P, Gong F, et al. (2025) A Bayesian-physical informed conditional tabular generative adversarial network framework for low-carbon concrete data augmentation and hyperparameter optimization. *Eng Appl Artif Intell* 152: 110811. https://doi.org/10.1016/j.engappai.2025.110811

42. Li M, Hao H, Shi YC, et al. (2018) Specimen shape and size effects on the concrete compressive strength under static and dynamic tests. *Constr Build Mater* 161: 84–93. https://doi.org/10.1016/j.conbuildmat.2017.11.069

43. Jin L, Yu W, Du X, et al. (2019) Mesoscopic numerical simulation of dynamic size effect on the splitting-tensile strength of concrete. *Eng Fract Mech* 209: 317–332. https://doi.org/10.1016/j.engfracmech.2019.01.035

44. Yan D, Qiu L, Wang J, et al. (2024) Dynamic damage constitutive model for UHPC with nanofillers at high strain rates based on viscoelastic dynamic constitutive model and damage evolution equation. *J Build Eng* 83: 108428. https://doi.org/10.1016/j.jobe.2023.108428

45. Shafighfard T, Kazemi F, Asgarkhani N, et al. (2024) Machine-learning methods for estimating compressive strength of high-performance alkali-activated concrete. *Eng Appl Artif Intell* 136: 109053. https://doi.org/10.1016/j.engappai.2024.109053

46. Kakasor Ismael Jaf D, Ismael Abdulrahman P, Salih Mohammed A, et al. (2023) Machine learning techniques and multi-scale models to evaluate the impact of silicon dioxide (SiO_2) and calcium oxide (CaO) in fly ash on the compressive strength of green concrete. *Constr Build Mater* 400: 132604. https://doi.org/10.1016/j.conbuildmat.2023.132604

47. Jin L, Yu WX, Du XL, et al. (2019) Meso-scale modelling of the size effect on dynamic compressive failure of concrete under different strain rates. *Int J Impact Eng* 125: 1–12. https://doi.org/10.1016/j.ijimpeng.2018.10.011

48. Wang S, Xia P, Gong F, et al. (2024) Multi objective optimization of recycled aggregate concrete based on explainable machine learning. *J Clean Prod* 445: 141045. https://doi.org/10.1016/j.jclepro.2024.141045

49. Zhang MH, Xu RH, Liu K, et al. (2022) Research progress on durability of marine concrete under the combined action of Cl^- erosion, carbonation, and dry-wet cycles. *Rev Adv Mater Sci* 61: 622–637. https://doi.org/10.1515/rams-2022-0049

50. Hemalatha T, Ramaswamy A (2017) A review on fly ash characteristics—Towards promoting high volume utilization in developing sustainable concrete. *J Clean Prod* 147: 546–559. https://doi.org/10.1016/j.jclepro.2017.01.114